Mora-Macias J (Orcid ID: 0000-0002-7997-9789)

1. Title page

Title: Comparison of methods for assigning the material properties of the distraction callus in computational models.

Juan Mora-Macías[a], Miguel Ángel Giráldez-Sánchez[b], Melchor López[c], Jaime Domínguez[d] and Esther Reina-Romo[d]

[a] University of Huelva. Department of Mining, Mechanical, Energy and Construction Engineering. Huelva (Spain). E-mail: juan.mora@dimme.uhu.es

[b] Virgen del Rocío Universitary Hospital. Clinical Orthopaedics, Trauma Surgery and Rheumatology Management Unit. Seville (Spain)

[c] Inerco Ingeniería. Seville (Spain)

[d] University of Seville. Department of Mechanical Engineering and Manufacturing. Seville (Spain).

Corresponding author: Juan Mora-Macías. Email: juan.mora@dimme.uhu.es. Phone: +34 959217322

This article has been accepted for publication and undergone full peer review but has not been through the copyediting, typesetting, pagination and proofreading process which may lead to differences between this version and the Version of Record. Please cite this article as doi: 10.1002/cnm.3227

2. Abstract and key terms

In silico models of distraction osteogenesis and fracture healing usually assume constant mechanical properties for the new bone tissue generated. In addition, these models do not always account for the porosity of the woven bone and its evolution. In this study, finite element analyses based on computed tomography (CT) are used to predict the stiffness of the callus until 69 weeks after surgery using 15 CT images obtained at different stages of an experiment on bone transport, technique in which distraction osteogenesis is used to correct bone defects Three different approaches were used to assign the mechanical properties to the new bone tissue. First, constant mechanical properties of the hard callus tissue and no porosity were assumed. Nevertheless, this approach did not show good correlations. Second, random variations in the elastic modulus and porosity of the woven bone were taken from previous experimental studies. Finally, the elastic properties of each element were assigned depending on gray scale in CT images. The numerically predicted callus stiffness was compared to previous *in vivo* measurements. It was concluded, firstly, that assignment depending on gray scale is the method that provides the best results and, secondly, that the method which considers a random distribution of porosity and elastic modulus of the callus is also suitable to predict the callus stiffness from 15 weeks after surgery. This finding provides a method for assigning the material properties of the distraction callus which does not require CT images and may contribute to improve current *in silico* models.

Key words: distraction osteogenesis, bone transport, callus stiffness, computerized tomography*, in vivo*, *in silico*.

3. Introduction

Similar to the fracture healing process, during distraction osteogenesis [1], woven bone grows within the distraction callus rapidly with a disorganized pattern, with the aim of providing temporary, rapid mechanical support. Assessing the mechanical properties of the distraction callus is important for evaluating the clinical evolution of the distraction osteogenesis process. The increasing stiffness of the tissues within the callus throughout the process represents the mechanical stability of the distracted bone. Therefore, information on the rate of increase of the callus mechanical properties will help to identify an endpoint of healing and may contribute to improving the current treatment strategies. This approach is of great importance since in the field of distraction osteogenesis, surgeons still lack established instructions to correctly define the specific patient planning of the process.

Several techniques have been developed to quantify bone healing in mechanical terms. However, the existing methods for assessing these callus mechanical properties are subjective and have some limitations. X-rays and manual clinical examinations, which are commonly used in daily clinical routines, have proven to be inexact [2-5] and cannot provide sufficient quantitative information. Assessment of the distraction callus stiffness *in vivo* using instrumented fixators provides suitable estimations of the callus stiffness [6-10]. However, it is not always convenient or possible to use external and instrumented fixators. In addition, with the last method, a stiffness measurement cannot be provided after distractor removal. On the other hand, methods to evaluate the callus mechanical properties *ex vivo* in animal experiments, such as nanoindentation [11-13] or mechanical testing of the whole specimen [14,15] involve having a group of animals that must be sacrificed at each time point of the evaluation.

Non-invasive methods have been used to assess the stiffness of the callus *in vivo*, such as high resolution magnetic resonance [16], quantitative ultrasound [17] and computational tomography (CT) images that are taken as the bases for finite element analyses [18]. Unlike the other techniques, prediction of the bone tissue mechanical properties by using CT images as the basis for finite element analysis has been assessed for reliability in the literature. Harp et al. [19] demonstrated that the stiffness of tubular bones, cortical and cancellous, can be accurately predicted by quantitative CT images. The bone mineral content in a fracture callus from CT images was correlated with experimental measurements of callus stiffness in a previous study [20]. The CT image finite element analysis method consists of obtaining an estimation of the stiffness of a bone tissue specimen using a finite element model that imports both three-dimensional geometry and the material properties of each element (depending on the gray scale values) from CT images. This method has been used in previous studies in mature bone tissue [21,22], reconstructed bones [23], trabecular bone [24,25], osteoporotic bone [26] and fracture callus [18]. However, as far as the authors know, CT image-based finite element analysis has not been used to estimate the stiffness of the callus during the distraction osteogenesis process.

Segmentation of CT images could also provide information about the tissue type percentages within the callus (soft and hard tissue) since they can be differentiated according to the gray scale. These manual sets of materials can be assigned the mechanical properties of the corresponding tissue type in finite element models. For example, in computational models of bone healing and distraction osteogenesis [27-31] the data available in the literature for tissue mechanical properties have been incorporated into each set of elements, corresponding to each tissue type. This approach can be appropriate for tissues that have constant properties throughout the

process and could be considered to be homogeneous from a certain scale, such as the cortical bone. However, the mechanical properties and porosity level are not constant with time for the other tissue types. For example, in the case of woven bone, it has been shown that the porosity and mechanical properties vary along the fracture healing [12] and distraction osteogenesis [13,32] processes.

The aim of this work is to provide and compare different estimations of the distraction callus stiffness during the process of bone transport by means of CT image-based finite element analysis. It was possible to estimate the callus stiffness until 69 weeks after surgery, increasing the time range of the *in vivo* measurements reported in the literature [10]. Finite element models were obtained from CT images that were obtained during an experiment in sheep [10]. Three different approaches were used to assign the elements' mechanical properties. In the first case, the mechanical properties were assigned manually to a model that was divided into four zones: hard callus tissue, soft callus tissue, cortical bone and bone marrow. Constant mechanical properties of the hard callus tissue and no porosity were assumed. In the second case, the mechanical properties of the hard callus tissue were taken from previous *in vivo* studies which provided the variations in the elastic modulus [13] and the porosity [32] of woven bone. In the third case, the elastic properties of each element were assigned depending on the level of Hounsfield Units (HU), regardless its location [18].

4. Materials and methods

Animal experiments

An experiment on bone transport was conducted in the metatarsus of 11 female merino sheep that were 3 to 5 years of age [10,33]. The bone transport process

consists of different phases. First, there is a latency phase of 7 days after surgery, in which the distractor was implanted. Second, a distraction period of 15 days, during which the bone segments were separated 1mm per day. Third, the consolidation phase extended until the distractor removal (153 ± 44 days from surgery), when the callus is totally ossified. Once, the distractor was removed, bone remodeling continued. The welfare of the animals during the experiments was guaranteed by the experimentation ethics committee of the University of Seville.

Three-dimensional models of the metatarsus

Fig. 1 shows the stages that were followed to numerically predict the stiffness of the distraction callus. To follow the whole process of bone consolidation, the distraction calluses were imaged with a CT scanner (General Electric, Hi Speed Dual) at different time points during the healing process. The resolution of the CT images was 200–300 μm/voxel. A total of 9 sheep were sacrificed, interrupting bone transport at different stages during the distraction and consolidation phases: 17, 22, 29, 35, 37, 51, 79, 98 and 161 days after surgery (to avoid artifacts caused by the metallic parts of the distractor during the CT images). The remaining two sheep were studied during the remodeling phase, after the distractor was removed and the callus had completely ossified. Therefore, these animals were not sacrificed, and several CT images were performed *in vivo* on them (137, 205, 277, 311, 379 and 471 days after surgery).

3D models were generated in the commercial program Mimics® (Materialise, Leuven, Belgium) from the 15 CT images obtained. From them, meshes were created in Ansys® (ANSYS Inc., Canonsburg, Pennsylvania, U.S.A), and the mechanical properties were assigned, as mentioned above, by three different methods: by manual segmentation with constant properties and no porosity, by manual segmentation with

in vivo data [13,32] or according to the HU [18]. The materials of each element of the model were assumed to be linear, elastic and isotropic.

Mechanical properties assignment: manual segmentation (MA).

In the first case, the elements of each model were divided into four zones according to their gray scale level in the CT images and their position within the callus: hard callus tissue, soft callus tissue, cortical bone and bone marrow (Fig. 1). The porosity was not accounted for, and the mechanical properties were considered to be constant over time according to the literature. The soft callus tissue region was assumed to be mainly granular tissue [34] and was assigned an elastic modulus of 2 MPa and Poisson coefficient of 0.13 [35,36]. The mechanical properties of the cortical bone were considered to be homogeneously distributed (E=17000 MPa, v =0.30) [37] as well as those of the medullar tissue (1 MPa, v =0.05) [35,36] and hard callus tissue (1000 MPa, v =0.29) [35,36].

Mechanical properties assignment: manual segmentation based on experiments (MAE).

In this case, the mechanical properties of the hard callus tissue (which involves the woven bone and some pores within the tissue) were not considered to be constant since a recent study showed that the mechanical properties [13] and porosity [32] of the hard callus tissue developed during bone transport vary with time. It was hypothesized that the mechanical properties of the hard callus tissue have more influence on the callus stiffness than the soft callus. Therefore, the mechanical properties of the soft callus tissue were considered to be constant, as in the MA case. The same constant values presented in MA were also considered for medullar and cortical bone tissues around the callus.

Fig. 2 shows the assignment scheme for the mechanical properties of the hard callus set of elements. First, the porosity level and range of the elastic modulus of the hard callus tissue were defined for each time point from the experiments. Fig. 2a shows the level of porosity extrapolated from measurements in Mora-Macías et al [32]. Fig. 2b shows the range of the elastic modulus extrapolated from measurements in Mora-Macías et al. [13], which were obtained for the solid matrix of the hard callus tissue (the woven bone). In both experiments, measurements were taken 35, 51, 79, 98, 161, and 525 days after surgery in some of the specimens that were scanned in this work (17, 22, 29, 35, 37, 51, 79, 98, 137, 161, 205, 277, 311, 379 and 471 days after surgery). The measurements were extrapolated linearly between 161 and 525 days after surgery. For 17, 22 29 and 37 days after surgery, the values at 35 days after surgery were assigned. As observed in Fig. 2c, the elements of the hard callus tissue set were reconsidered to be pore or solid matrix (since the CT resolution is lower than the porous and trabecular sizes observed experimentally, Fig. 2d). A random distribution was chosen to select the pore elements and solid elements according to the level of porosity measured at each time point (Fig. 2a). The pore elements were assigned the mechanical properties defined for the soft callus tissue (E = 2 MPa). The solid elements were considered to be woven bone with an elastic modulus randomly assigned within the range defined in Fig. 2b for each time point, and a Poisson coefficient of 0.3 was used. For example, in the case of the model generated from the CT images taken 98 days after surgery, in the hard callus set of elements, 49.5% of the elements were considered to be pores and 50.5% were considered to be solid matrix (Fig. 2a). The elements that were considered to be solid matrix were randomly assigned an elastic modulus within the range 3 to 15 GPa (Fig. 2b).

Mechanical properties assignment: HU segmentation (HU)

In the third case, the mechanical properties of each element of the model were assigned according to their particular level of HU in the CT images. The relationship elastic modulus-gray value used by Shefelbine et al. [18] for a fracture healing case study was adapted by extrapolating the gray values to HU units, which were expressed as a percentage of the maximum HU level in each CT to obtain normalized results (Fig. 3a). The soft tissue (gray values < 48, HU<33%) had a constant elastic modulus of 50 MPa [18]. The hard tissue elastic modulus depended on the gray value/HU linearly, increasing from 50 MPa (gray value= 48, HU=33%) to 18 GPa (gray value=127, HU=95%). In addition, to account for cortical bone (not modeled in Shefelbine et al. [18]), elements with an HU level of above 95% of the maximum HU level were considered to be fully mineralized and were assigned the same elastic modulus as the maximum value for the hard callus tissue (18 GPa). Fig. 3b shows the model 50 days after surgery once the mechanical properties using this method were assigned; the colors represent the elastic modulus of each element from the minimum values for the soft tissues (blue) to the maximum for the cortical bone (red).

Callus stiffness prediction, loading and boundary conditions

Simulations were performed in Abaqus® (Sassault Systemes, Vélizy-Villacoublay, France). The boundary conditions of the model consisted of constraining the distal segment of bone (Fig. 4a). The loading conditions consisted of a force applied to the proximal segment. The values were taken from those measured experimentally *in vivo* for each day of the distraction process according to Mora-Macías et al. [10] (Fig. 4b). These loading and boundary conditions simulate the mechanical conditions in the callus stiffness that cause compression of the metatarsus during gait [10]. For each

time point, the model was simulated with the corresponding load and the displacements were calculated. A prediction of the callus stiffness was obtained for the simulation in each case by taking the applied compression force divided by the difference in the distance in the longitudinal direction between the nodes that corresponded to the distal and proximal cortical bone segments around the callus (red dotted lines in Fig. 4a).

5. Results

Fig. 5 shows the predictions of the callus stiffness that were obtained with the different mechanical properties assignments described above.

Mechanical properties assignment: manual segmentation (MA)

If the porosity of woven bone is not considered and constant mechanical properties are assumed, the predictions of the callus stiffness increase from values under 3 kN/mm to values around 50 kN/mm during the bone transport process (Figs. 5a and 5b). Comparing the callus stiffness predictions using the other methods, manual segmentation predicts lower values of the callus stiffness at the end of the process, but higher values at the beginning of the process (Fig. 5b).

Mechanical properties assignment: manual segmentation-based experiments (MAE)

In this case, the callus stiffness prediction presented in Fig. 5 is the mean of 5 different simulations. Performing 5 different simulations aims to evaluate the possible variations in the random distributions used to assign the mechanical properties of the hard callus tissue. Table 1 shows the coefficient of variation of these five predictions for each time point. According to this table, no significant variations were observed among the 5 predictions for each time point.

According to the mean values of the callus stiffness predicted in Fig. 5a, it increases from approximately 1 to values around 220 KN/mm after 300 days from surgery. These predicted values are in accordance with the HU predictions after 100 days from surgery. However, at the beginning of the process, the predictions are closer to those values obtained for the MA assignment (Fig. 5b).

Mechanical properties assignment: HU

Fig. 5a shows the callus stiffness predictions obtained in the case of assigning mechanical properties according to the level of HU. The results predicted an increase in callus stiffness from values under 1 kN/mm to values around 180 kN/mm during the bone transport process. Additionally, the callus stiffness predictions seems according to the experimental values measured until 80 days after surgery (Fig. 5b).

Hard / soft tissue evolution within the distraction callus

CT images performed also provide results about the volume distribution of the tissue within the callus. Fig. 6 shows that for the first specimens, directly after the distraction phase, the proportion of hard and soft callus tissue is similar. Afterward, the volume of hard tissue increases at the same time that the volume of soft tissue decreases. From around 90 days after surgery, most of the callus is ossified and the percentage of hard callus tissue is above 80%. As it will be discussed below, the percentage of soft and hard tissue within the callus may explain the results obtained in the three different simulations carried out

6. Discussion

In this work, the mechanical properties of the distraction callus over time were evaluated *in silico* based on CT images. Three different approaches were used to assign the mechanical properties to the tissues that developed within the distracted callus (simple manual segmentation, manual segmentation based on experiments or segmentation based on the level of HU) and were compared with *in vivo* measurements.

Fig. 7a shows the callus stiffness predictions by the three methods used versus the mean value of the callus stiffness measured *in vivo* (until 80 days from surgery). The assignment of mechanical properties according to the level of HU (R^2 = 0.9719) provided more accurate results compared to the MA and MAE predictions (R^2 = 0.6255 and 0.6151 respectively). The fact that more accurate results were provided by assignment according to the level of HU could be due to the imposition of a border between the soft and hard callus tissues, which was due to manual segmentation. Until 80 days after surgery, an important part of the callus is soft tissue (Fig. 6). Manual segmentation does not allow the areas in which soft and callus tissues are mixed to be simulated. However, 100 days after surgery, MAE assignment was useful for providing an acceptable estimation of the callus stiffness evolution, which is close to the HU prediction (R^2 = 0.9614), as shown in the correlation between the results of the prediction of the callus stiffness using assignment according to the level of HU (Fig. 7b). Additionally in Fig. 7b, it can be observed that the MA assignment does not provide results as in concordance with HU predictions as MAE (R^2 = 0.8422).

Homogeneous sets of elements that represent different tissue types (e.g., medullar tissue, cortical bone soft and hard callus tissue) have been traditionally used in

mechanobiological studies of distraction osteogenesis and bone healing while assigning constant properties to each set of elements [27-31]. However, this approach uses a strong assumption since the mechanical properties of all tissue types within the callus increase during the distraction phase [1,13,38]. Manual segmentation conducted in this study accounts for the variation in the mechanical properties of the hard callus tissue taken from experiments [13,32]. The proposed random distribution of the porosity and elastic modulus of woven bone provides acceptable predictions of the callus stiffness compared with *in vivo* measurements and the assignment of mechanical properties according to the level of HU (Fig. 7). Therefore, this distribution of the porosity and elastic modulus of woven bone could be used in future mechanobiological studies of distraction osteogenesis and bone healing. As far as the authors know, this study is the first time that experimental data of the evolution of the porosity and elastic modulus of woven bone have been used to assign material properties in computational models of distraction osteogenesis.

In general, all of the methods predicted lower values of stiffness at the end of the process (from 10 to 100 kN/mm approximately between 350 and 450 days) compared with the maximum values (from 150 to 250 kN/mm between 150 and 300 days). It was observed in all of the cases studied that the stiffness decreased after achieving a peak value between 150 and 300 days after surgery, approximately (Fig. 5a). This finding has been suggested previously in other studies in the literature [39]. However, more time points after 471 days after surgery are necessary to consider this suggestion to be a definitive result.

According to a previous study that used the same samples [10], the volume (and also the mean compression area) of the callus grows during the consolidation phase until

it achieves a peak. Afterwards, the callus volume decreases due to the bone resorption process that takes place during the remodeling phase, the medullary canal is created and the mean callus area is reduced. This may explain the evolution of the callus stiffness since callus stiffness depends on the geometry (Fig. 5). To avoid the influence of the geometry, a mean elastic modulus of the callus has been estimated by multiplying the values of the callus stiffness reported by the length and dividing by the callus area (Fig. 8). Fig. 8 shows the evolution of the mechanical properties of the callus (mean elastic modulus of the materials which make up the callus: woven bone and soft tissues). It may be observed in figure 2 that the mean elastic modulus of the callus increases during all the process of distraction unlike callus stiffness.presents several limitations and assumptions that must at least be revised to understand their implications. First, in the manual segmentation procedure, only four different tissue types were differentiated: soft callus tissue, hard callus tissue, cortical bone and bone marrow. Second, all of the tissues were assumed to be linear, elastic and isotropic. Additionally, the callus stiffness was evaluated under the small deformation assumption. Third, the numerical values were compared against *in vivo* experimental data until day 79 after surgery. Fourth, the callus stiffness estimations showed significant values of scatter for all of the cases analyzed (Fig. 5a), especially at the end of the process. This scatter is due to the inter-individual differences during the process. For example, Fig. 5a shows that the stiffness of the callus at 137, 205 and 311 days from surgery (time points from the same animal) is approximately three times the callus stiffness at 277, 379 and 471 days from surgery (time points from a different animal). This finding is due to the difference in volume of the callus of both animals that can be observed in 3D reconstructions (Fig. 9 [10]). Fig. 8 also shows that inter-individual differences are mainly due to callus geometry differences since the level of

scatter is lower in the evolution of the mean elastic modulus compared to the callus stiffness, which depends on geometry. Finally, the assumption of constant and uniform mechanical properties for the soft callus tissue in the manual segmentations implies that the soft callus tissue could not vary its mechanical properties along the bone transport process and contradicts the high scatter elastic modulus of the soft callus tissue measured in the literature [11]. This limitation could explain that a more accurate result was provided by assignment according to the level of HU (Fig. 7a).

As far as the authors know, this model is the first to evaluate the stiffness of the callus computationally during distraction osteogenesis. The described procedures for assigning the mechanical properties can be very useful in improving future *in silico* models and current clinical protocols. For example, it is critical for clinicians to decide the moment when the fixator must be removed without stiffness measurements. In fact, a premature fixator removal is usually a source of complications [40,41].

7. Acknowledgments

The authors gratefully acknowledge the Ministerio de Economía y Competitividad del Gobierno España (DPI2014-58233-P and DPI2017-82501-P) for research funding. The authors are also grateful to the University of Zaragoza for its collaboration. Importantly, we also thank J. Morgaz from the University of Córdoba as well as M. López-Pliego from the Virgen del Rocío Hospital (Seville) for their contributions.

8. Disclosure of potential Conflicts of Interests

Authors AI and IJ declare that they have no conflict of interest.

9. Research Involving Human Participants/Animals

N/A.

10. Informed consent
N/A.

11. References

[1] Ilizarov G. A. The tension-stress effect on the genesis and growth of tissues: Part II. The influence of the rate and frequency of distraction. Clinic Orthop Relat Res. 239: 263–285, 1989.

[2] Hammer R. R., S. Hammerby, and B. Lindholm. Accuracy of radiologic assessment of tibial shaft fracture union in humans. Clinic Orthop Relat Res. 199:233-8, 1985.

[3] Panjabi M. M., R. W. Lindsey, S. D Walter, and A. A. White 3rd. The clinician's ability to evaluate the strength of healing fractures from plain radiographs. J Orthop Trauma, 3:29–32, 1989.

[4] Panjabi M. M., S. D. Walter, M. Karuda, A. A. White, and J. P. Lawson. Correlations of radiographic analysis of healing fractures with strength: a statistical analysis of experimental osteotomies. J. Orthop. Res. 3:212–218, 1985.

[5] Webb J., G. Herling, T. Gardner, J. Kenwright, and A. H. Simpson. Manual assessment of fracture stiffness. Injury, 27:319–320, 1996.

[6] Aarnes G. T., H. Steen, P. Ludvigsen, N. A. Waanders, R. Huiskes, and S. A. Goldstein. In vivo assessment of regenerate axial stiffness in distraction osteogenesis. J Orthop Res. 23:494–498, 2005.

[7] Dwyer J. S., P. J. Owen, G. A. Evans, J. H. Kuiper, and J. B. Richardson. Stiffness measurements to assess healing during leg lengthening. A preliminary report. J Bone Joint Surg. Br. 78:286–289, 1996.

[8] Floerkemeier T., W. Aljuneidi, J. Reifenrath, N. Angrisani, D. Rittershaus, D. Gottschalk, S. Besdo, A. Meyer-Lindenberg, H. Windhagen, and F. Thorey. Telemetric in vivo measurement of compressive forces during consolidation in a rabbit model. Technol Health Care. 19:173–183, 2011.

[9] Mora-Macías J., E. Reina-Romo, and J. Domínguez. Distraction osteogenesis device to estimate the axial stiffness of the callus in Vivo. Med Eng Phys. 37:969-78,2015.

[10] Mora-Macías J., E. Reina-Romo, M. López-Pliego, M. A. Giráldez-Sánchez, and J. Domínguez. In vivo mechanical characterization of the distraction callus during bone consolidation. Ann Biomed Eng. 43:2663-74, 2015.

[11] Leong P. L., and E. F. Morgan. Measurement of fracture callus material properties via nanoindentation. Acta Biomater. 4:1569–1575, 2008.

[12] Manjubala I., Y. Liu, D. R. Epari, P. Roschger, H. Schell, P. Fratzl, and G. N. Duda. Spatial and temporal variations of mechanical properties and mineral content of the external callus during bone healing. Bone. 45:185–192, 2009.

[13] Mora-Macías J., A. Pajares, P. Miranda, J. Domínguez, and E. Reina-Romo. Mechanical characterization via nanoindentation of the woven bone developed during bone transport. J Mech Behav Biomed Mater. 74:236-244, 2017.

[14] Floerkemeier T., F. Thorey, C. Hurschler, M. Wellmann, F. Witte, and H. Windhagen. Stiffness of callus tissue during distraction osteogenesis. Orthop Traumatol Surg Res. 96:155–160, 2010.

[15] Ohyama M., Y. Miyasaka, M. Sakurai, A. T. Yokobori, and Jr, S. Sasaki. The mechanical behavior and morphological structure of callus in experimental callotasis. Biomed Mater Eng. 4:273–281, 1994.

[16] Liu X. S., X. H. Zhang, C. S. Rajapakse, M. J. Wald, J. Magland, K. K. Sekhon, M. F. Adam, P. Sajda, F. W. Wehrli, and X. E. Guo. Accuracy of high-resolution in vivo micro magnetic resonance imaging for measurements of microstructural and

mechanical properties of human distal tibial bone. J Bone Mineral Res. 25:2039–2050, 2010.

[17] Raum K., I. Leguerney, F. Chandelier, E. Bossy, M. Talmant, A. Saied, F. Peyrin, and P. Laugier. Bone microstructure and elastic tissue properties are reflected in QUS axial transmission measurements. Ultrasound Med. Biol. 31:1225–1235, 2005.

[18] Shefelbine S. J., U. Simon, L. Claes, A. Gold, Y. Gabet, I. Bab, R. Müller, and P. Augat. Prediction of fracture callus mechanical properties using micro-CT images and voxel-based finite element analysis. Bone. 36:480–8, 2005.

[19] Harp J. H., J. Aronson, and M. Hollis. Noninvasive determination of bone stiffness for distraction osteogenesis by quantitative computed tomography scans. Clinic Orthop Relat Res. 301:42–8, 1994.

[20] Augat P., J. Merk, H. K. Genant, and L. Claes. Quantitative assessment of experimental fracture repair by peripheral computed tomography. Calcif Tissue Int, 60:194–9, 1997.

[21] Cattaneo P. M., M. Dalstra, and L. H. Frich. A three-dimensional finite element model from computed tomography data: a semi-automated method. Proc Inst Mech Eng H. 215:203–13, 2001.

[22] Gupta S., F. C. T. van der Helm, J. C. Sterk, F. van Keulen, and B. L. Kaptein. Development and experimental validation of a three-dimensional finite element model of the human scapula. Proc Inst Mech Eng H. 218:127–42, 2004.

[23] Taddei F., M. Viceconti, M. Manfrini, and A. Toni. Mechanical strength of a femoral reconstruction in paediatric oncology: a finite element study. Proc Inst Mech Eng H. 217:111–9, 2003.

[24] Müller R., and P. Rüegsegger. Three-dimensional finite element modelling of non-invasively assessed trabecular bone structures. Med Eng Phys. 17:126–33, 1995.

[25] Van Rietbergen B., H. Weinans, R. Huiskes, and A. Odgaard. A new method to determine trabecular bone elastic properties and loading using micromechanical finite-element models. J. Biomech, 28:69–81, 1995.

[26] Newitt D. C., S. Majumdar, B. van Rietbergen, G. von Ingersleben, S. T. Harris, H. K. Genant, C. Chesnut, P. Garnero, and B. MacDonald. In vivo assessment of architecture and micro-finite element analysis derived indices of mechanical properties of trabecular bone in the radius. Osteoporos Int. 13:6–17, 2002.

[27] Gómez-Benito M. J., J. M. García-Aznar, J. H. Kuiper, and M. Doblaré. Influence of fracture gap size on the pattern of long bone healing: a computational study. J.Theor. Biol. 235:105-119, 2005.

[28] Isaksson H., O. Comas, C. C. Van Donkelaar, J. Mediavilla, W. Wilson, R. Huiskes, and K. Ito. Bone regeneration during distraction osteogenesis: mechano-regulation by shear strain and fluid velocity. J. Biomech. 40:2002-11, 2007.

[29] Reina-Romo E., M. J. Gómez-Benito, A. Sampietro-Fuentes, J. Domínguez, and J. M. García-Aznar. Three-Dimensional Simulation of Mandibular Distraction Osteogenesis: mechanobiological Analysis. Ann. Biomed. Eng. 39:35-43, 2011.

[30] Reina-Romo E., M. J. Gómez-Benito, J. Domínguez, F. Niemeyer, T. Wehner, U. Simon, and L. E. Claes. Effect of the fixator stiffness on the young regenerate bone after bone transport: computational approach. J Biomech. 44:917–923, 2011.

[31] Reina-Romo E., M. J. Gómez-Benito, J. Domínguez, and J. M. García-Aznar. A lattice-based approach to model distraction osteogenesis. J Biomech. 45: 2736-42, 2012.

[32] Mora-Macías J., A. Pajares, P. Miranda, P. García Florencio, J. Domínguez, and E. Reina-Romo. Mechanical properties of the woven bone: effect of the porosity and mineralization. Ann. Biomed. Eng. UNDER REVIEW, 2018

[33] Mora-Macías J., E. Reina-Romo, J. Morgaz, and J. Domínguez. In vivo gait analysis during bone transport. Ann Biomed Eng. 43:2090-100, 2015.

[34] López-Pliego E. M., M. A. Giráldez-Sánchez, J. Mora-Macías, E. Reina-Romo, and J. Domínguez. Histological evolution of the regenerate during bone transport: an experimental study in sheep. Injury. 47:S7-S14, 2016.

[35] Reina-Romo E. Distraction osteogenesis: mechanobiological modeling and numerical applications. PhD Thesis, 2010.

[36] Reina-Romo E., M. J. Gómez-Benito, J. M. García-Aznar, J. Domínguez, and M. Doblaré. Growth mixture model of distraction osteogenesis: effect of pre-traction stresses. Biomech. Model. Mechanobiol. 9:103-15, 2010.

[37] Martin R. B., D. B. Burr, and N. A. Sharkey. Skeletal Tissue Mechanics. 1998.

[38] Mora-Macías J., E. Reina-Romo, and J. Domínguez. Model of the distraction callus tissue behavior during bone transport based in experiments in vivo. J Mech Behav Biomed Mater. 61:419-30, 2016.

[39] Aronson J., W. R. Hogue, C. M. Flahiff, G. G. Gao, X. C. Shen, R. A. Skinner, T. M. Badger, and C. K. Lumpkin. Development of tensile strength during distraction osteogenesis in a rat model. J Orthop Res. 19:64–9, 2001.

[40] Burke N. G., A. J. Cassar-Gheiti, J. Tan, G. McHugh, B. J. O'Neil, M. Noonan, and D. Moore. Regenerate bone fracture rate following femoral lengthening in paediatric patients. J Child Orthop. 11:210-215, 2017.

[41] Ilizarov G. A. Clinical application of the tension-stress effect for limb lengthening. Clinic Orthop Relat Res. 250:8-26, 1990.

Table 1. Coefficient of variation (COV) for the 5 callus stiffness predictions for each time point in the MAE simulations

Days from surgery	17	22	29	35	37	50	79	98	137	161	205	277	311	379	471
COV (%)	7.0	3.1	4.8	3.0	4.0	1.9	1.8	1.0	0.8	0.2	0.8	0.3	0.7	0.4	0.2

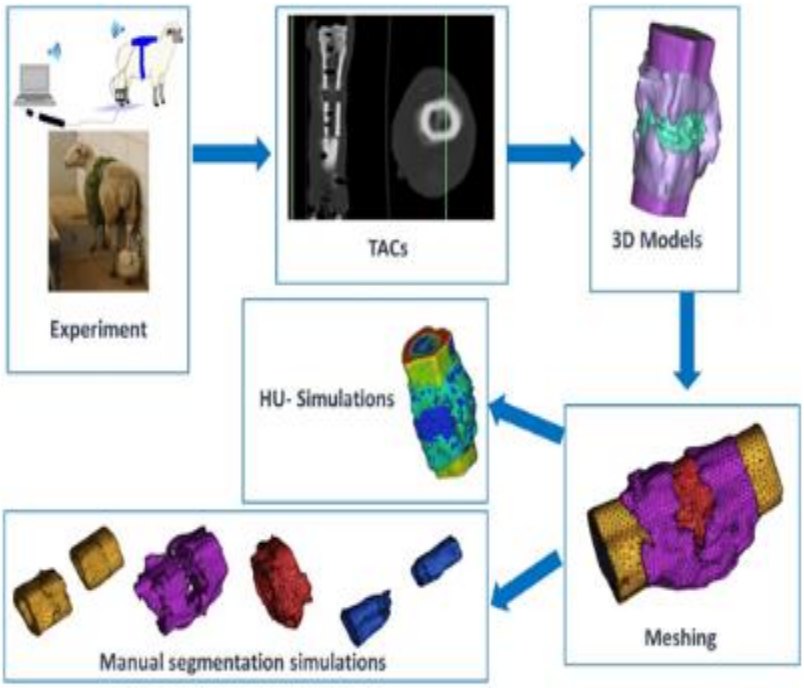

Fig. 1. General scheme of the steps followed to predict the stiffness of the distraction callus: animal experiment, computerized tomography, generation of 3D models, meshing and assignment of mechanical properties: according to manual segmentations or according to the level of HU.

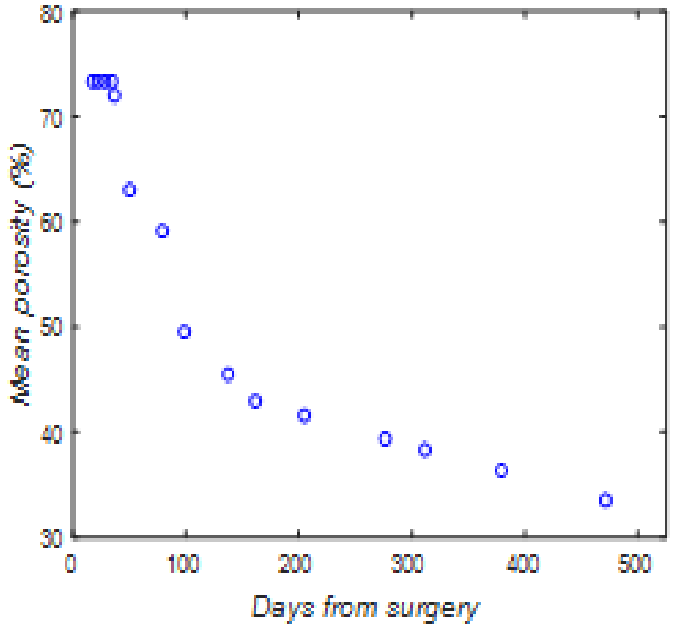

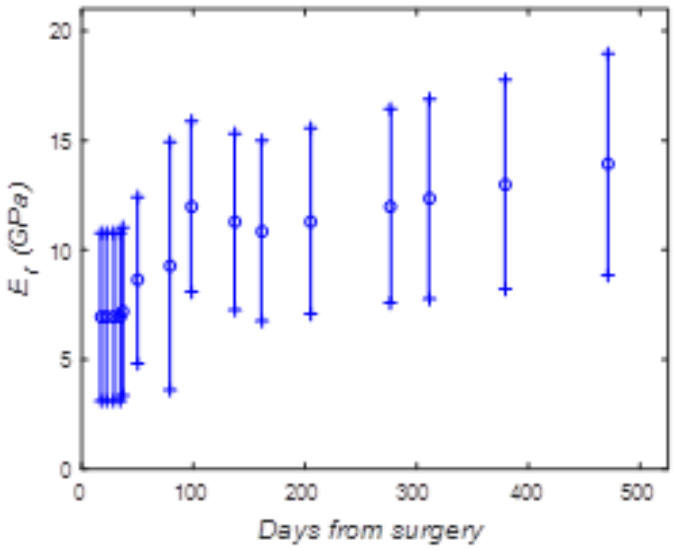

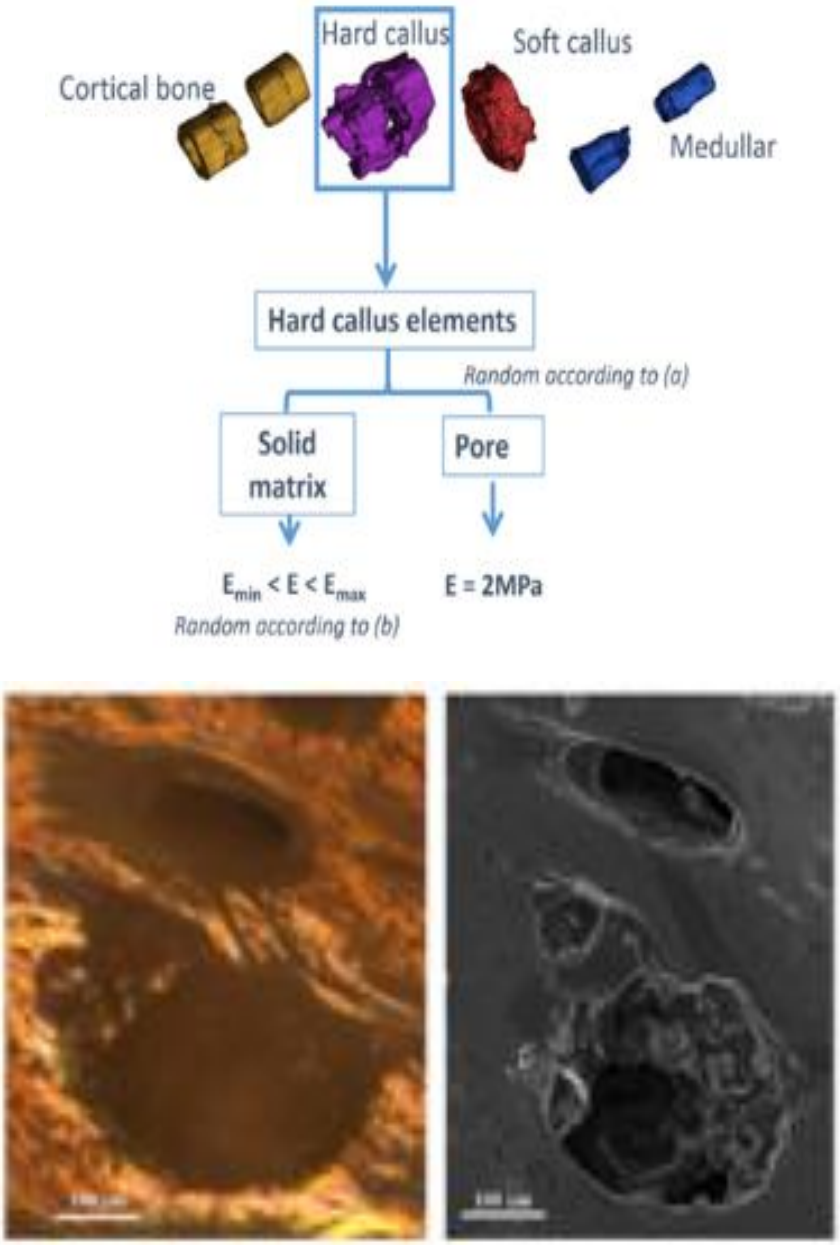

Fig. 2. (a) Level of porosity assigned to each time point analyzed in this work, extrapolated from the experimental measurements in Mora-Macías et al., 2018 [26]. (b) Range of elastic modulus assigned to each time point analyzed in this work, extrapolated from the experimental measurements in Mora-Macías et al., 2017 [13]. (c) Scheme of the assignment of mechanical properties of the hard callus tissue in manual segmentation. The elements of the hard callus set were classified as solid matrix or pore randomly according to (a). Afterward, an elastic modulus within the corresponding range (b) was assigned, also randomly, to those elements considered

to be solid matrix. Pore elements were considered to be soft callus tissue and were assigned with the same mechanical properties (E = 2 MPa). (d) Example of a porous area within the hard callus tissue, optical and scanning electron microscope images [13].

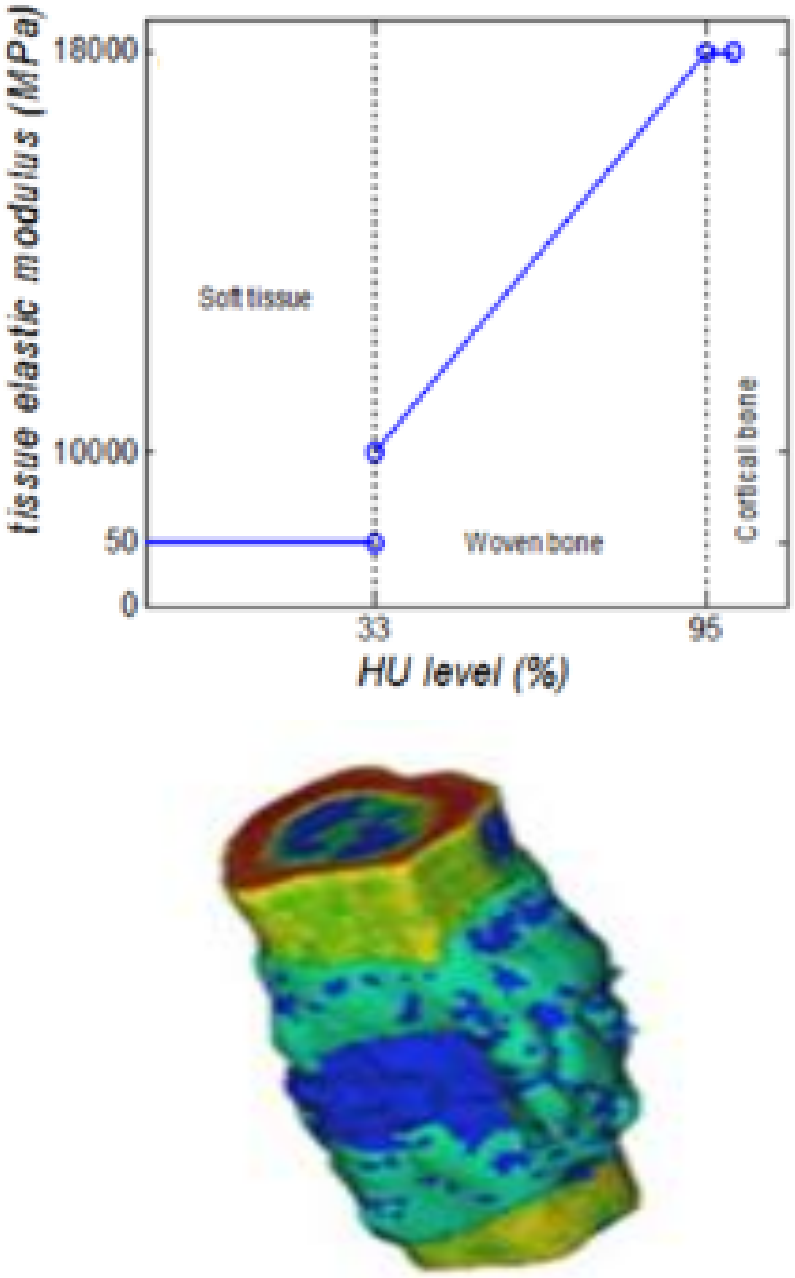

Fig. 3. (a) Relation between the tissue elastic modulus and the level of HU (% of the maximum value in the CT), adapted from Shefelbine et al., 2005. (b) Model of the callus 50 days after surgery after assigning the mechanical properties using this method; the colors represent the elastic modulus of each element from the minimum values for the soft tissues (blue) to the maximum for the cortical bone (red).

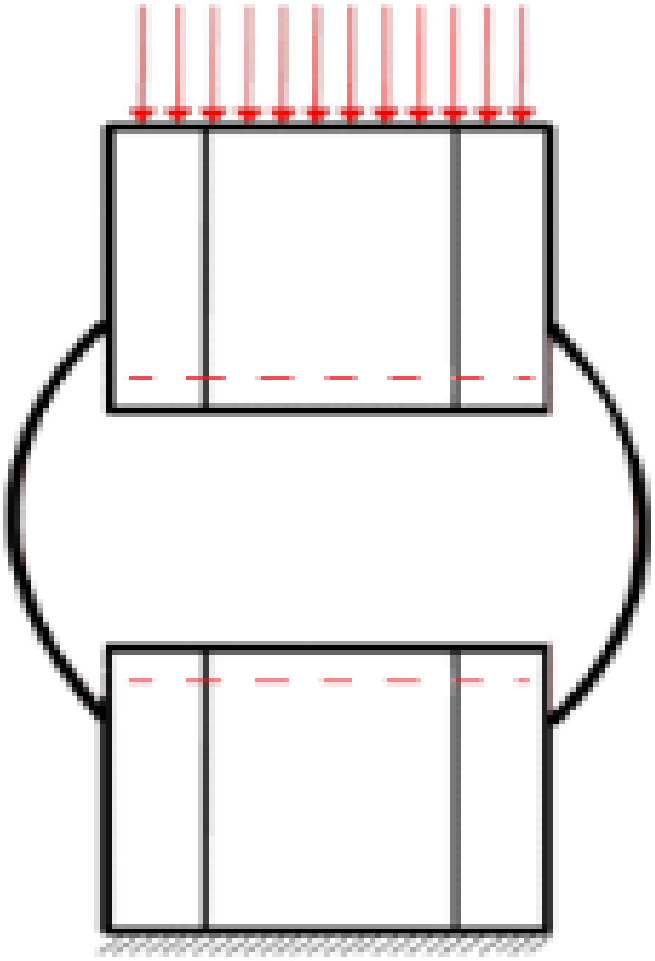

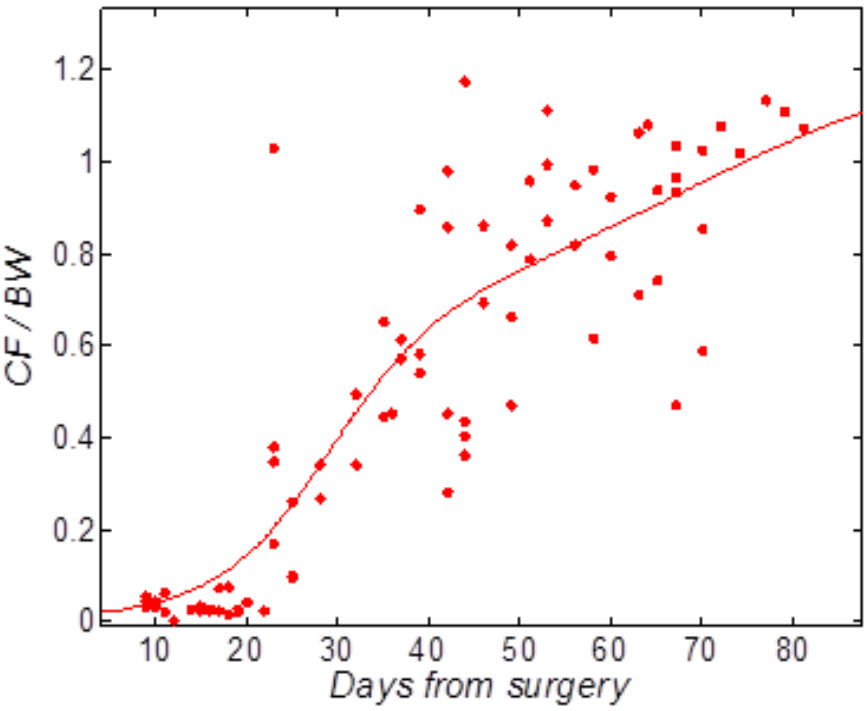

Fig. 4. (a) Scheme of the loading and boundary conditions. The red dotted lines represent the positions of the nodes whose displacements were used to calculate the

callus stiffness. (b) *In vivo* loading values versus the time in days after surgery (Mora-Macías 2015 b). The points are experimental values of the force through the callus (CF) with respect to the body weight (BW), and the line represents the fit of these values with time.

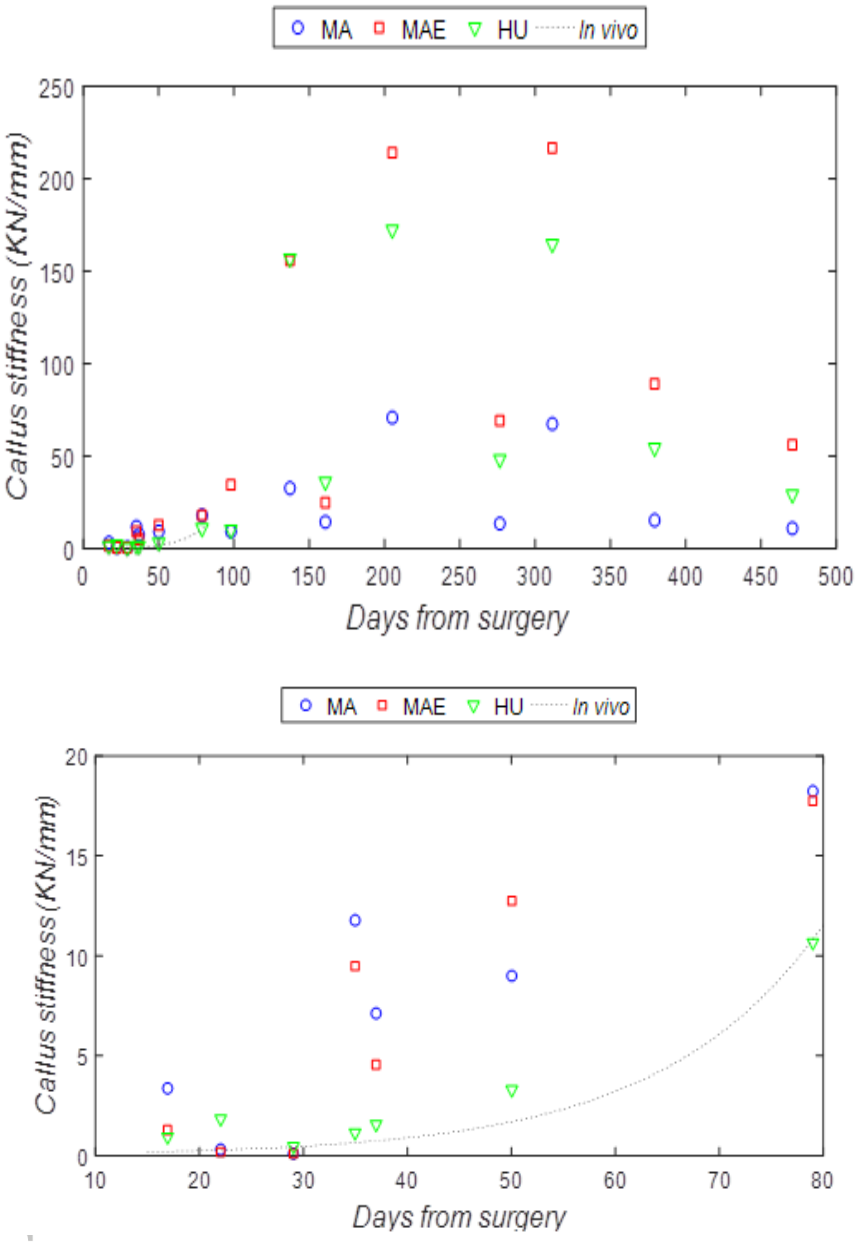

Fig. 5. (a) Predictions of the callus stiffness in the case of simple manual segmentation (MA), manual segmentation-based experiments (MAE) and in the case of assignment of mechanical properties according to the level of HU (HU). This figure also shows the fit of the callus stiffness values measured *in vivo* (dotted line) (b) Detailed view of the values before 100 days from surgery.

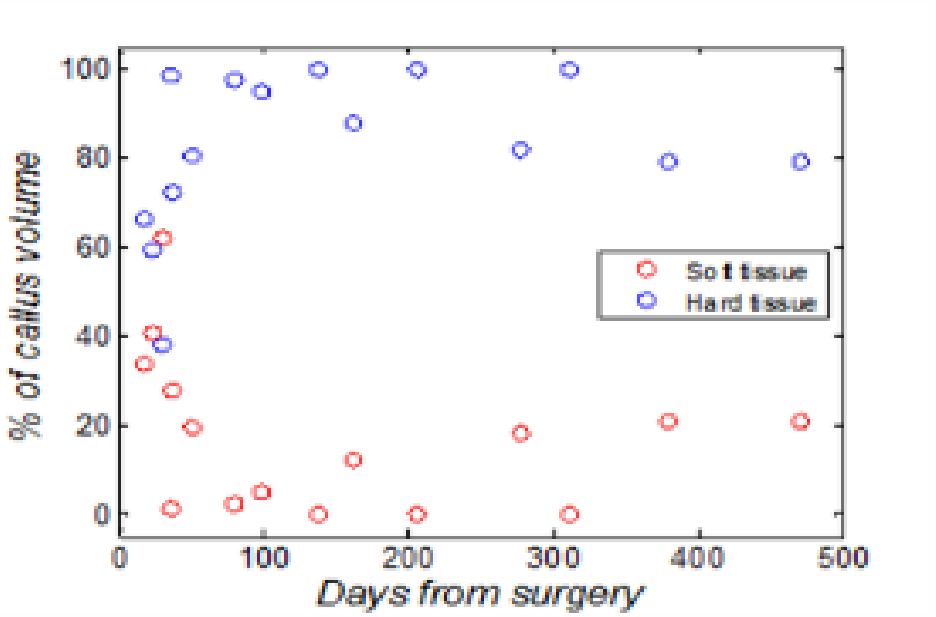

Fig. 6. Volume proportion of the soft and hard tissue within the callus from manual segmentation.

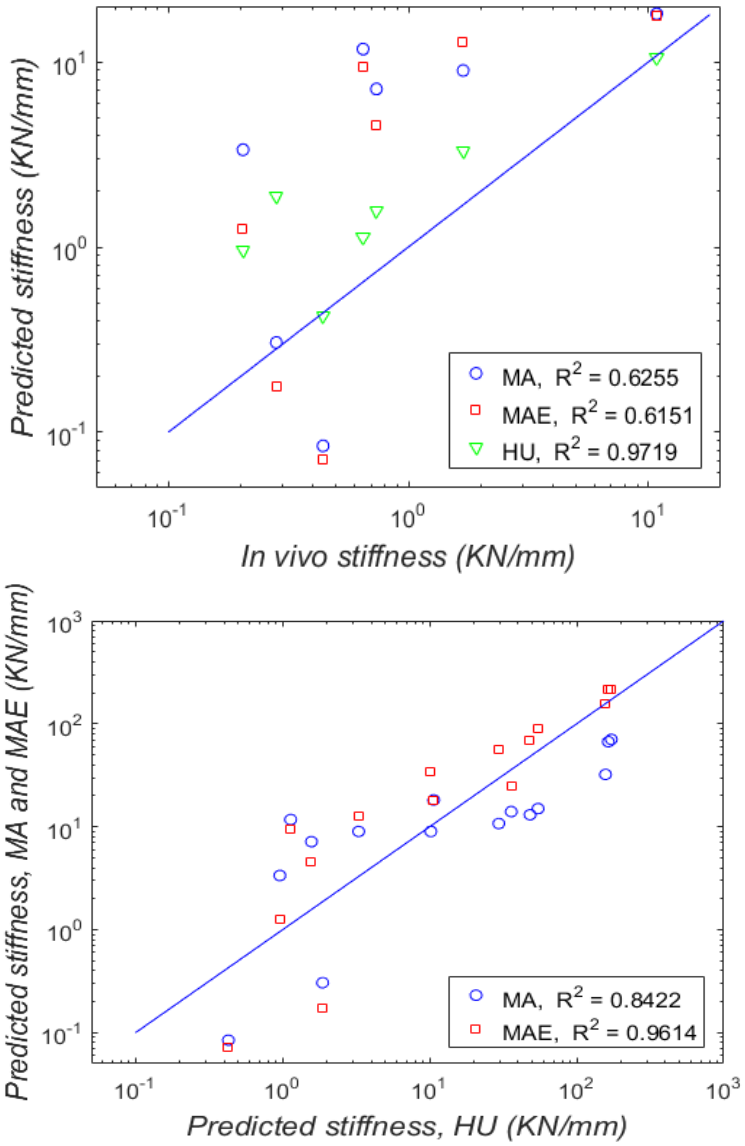

Fig. 7. (a) Predicted callus stiffness until 80 days after surgery for the methods used (mechanical properties assignment according to simple manual segmentation (MA), manual segmentation-based experiments (MAE) and according to the level of HU (HU)) versus the measured callus stiffness in vivo (Mora-Macías et al, 2015b). The line represents the ideal position of the points represented if the predictions of the callus stiffness for each time point would coincide with the value of the callus stiffness measured in vivo. (b) Predicted callus stiffness MA and MAE versus HU. The line represents the ideal position of the points represented if the predictions would give the same values.

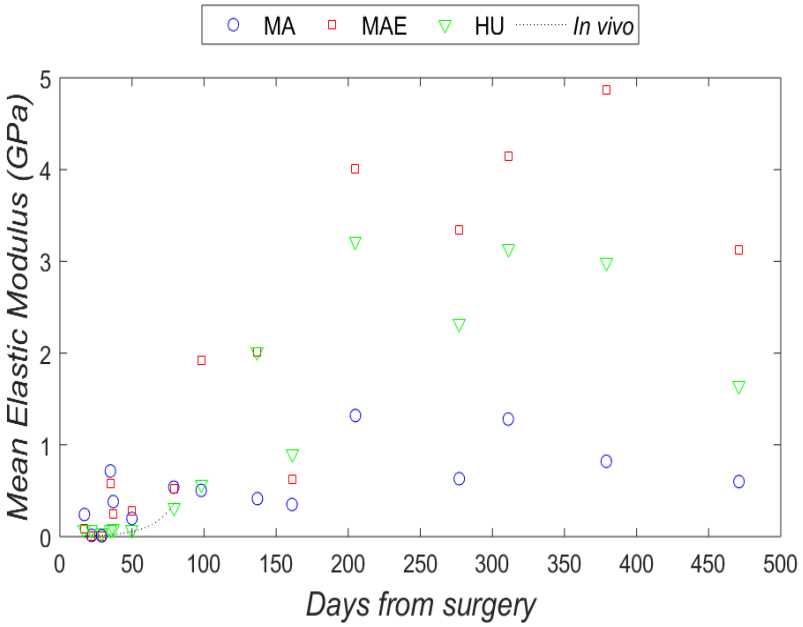

Fig. 8. Mean elastic modulus of the callus estimated from predictions of the callus stiffness in the case of simple manual segmentation (MA), manual segmentation-based experiments (MAE) and in the case of assignment of mechanical properties according to the level of HU (HU). This figure also shows the mean elastic modulus of the callus estimated from the callus stiffness values measured in vivo (dotted line)

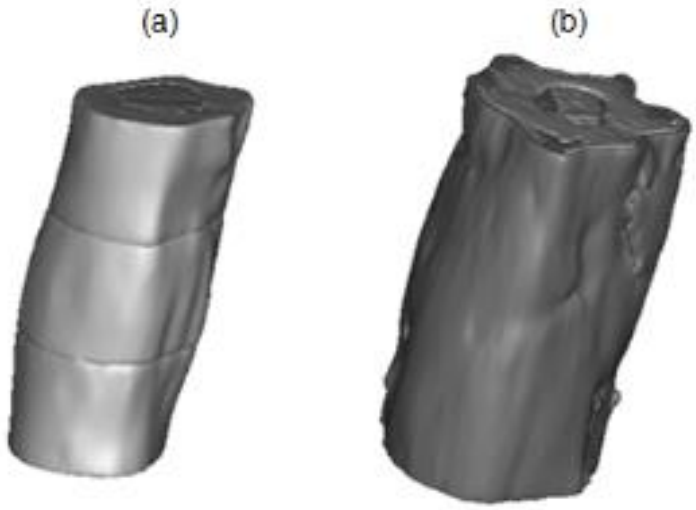

Fig. 9. 3D reconstruction of the callus and bone segments around (a) sheep number 5 scanned 277, 379 and 471 days after surgery and (b) sheep number 10 scanned 137, 205 and 311 days after surgery